



Original Article

## Deposition pattern of stony and muddy debris flow at the confluence area

**DU Cui**  <https://orcid.org/0000-0003-2892-1517>;  e-mail: ducui0125@163.com

*School of civil engineering, Henan University of Science and Technology, Luoyang 471023, China*

**Citation:** Du C (2021) Deposition pattern of stony and muddy debris flow at the confluence area. *Journal of Mountain Science* 18(3). <https://doi.org/10.1007/s11629-020-6046-y>

© Science Press, Institute of Mountain Hazards and Environment, CAS and Springer-Verlag GmbH Germany, part of Springer Nature 2021

**Abstract:** Debris flow fan affects the river profile and landscape evolution. The propagation of multiple debris flows along a river can cause inundation and breaching risk, which can be exemplified by the Min River after the Wenchuan earthquake, Sichuan province, China. In this work, large flume tests were conducted to examine the interactions between debris flows and water current with the fan geometry, momentum, runout distance, deposited width, the relative water level upstream and dominated stress. The results reveal that stony flow commonly travels at a high speed and forms a long rectangle shape fan, while the muddy flow generally travels at a low speed and forms a fan-shaped depositional area. The stony flow can block a river even when the momentum is close to the water current; the muddy flow can block a river when the momentum is lower than that of water current. In case of complete river damming, the relative water level upstream indicates that the inundation risk from the muddy flow damming river would be higher than the inundation risk of stony flow. The diversion ratio of muddy flow decreases as damming ratio. Comparison of dimensionless numbers reveals that stony flow is dominated by grain collision stress combined with turbulent mixing stress, while the muddy flow is dominated by viscous shear stress over friction stress. The fan geometry, damming ratio, diversion ratio, and the dominated stress all together indicate that stony flow strongly interacts with water current while the muddy flow does not. The results can be helpful for understanding the physical interactions between water current and various debris flows, and debris flow dynamics at the channel confluence area.

**Received:** 26-Feb-2020

**Revised:** 03-Apr-2020

**Accepted:** 26-Nov-2020

**Keywords:** Stony flows; Muddy flows; Physical interactions; Damming ratio; Dominated stress

### 1 Introduction

Debris flows generally initiate from discrete landslides (Iverson 2000; Gabet and Mudd 2006; Montrasio et al. 2009), or mobilize from channel bed failures (Gregoretti and Fontana 2010; Ma et al. 2018). They have strong sediment entrainment ability and are extremely destructive (Iverson et al. 2010; Kean et al. 2015). Debris flows often deliver tremendous sediments downstream and block a river, causing risk of inundation and outburst flood (Cui et al. 2013a; Du et al. 2014; Braun et al. 2018). In earthquake-stricken or fire-burned regions, the damages from subsequent debris flows are more serious than prior events (Tang et al. 2011; Santi and Morandi 2013; Tang et al. 2019).

Debris flows have various classifications depending on their appearance, sediment concentration, hydraulic features, viscosity, or a combination of them (Coussot and Meunier 1996; Cui et al. 2005; Imaizumi et al. 2011; Okano et al. 2012; Takahashi 2014). Among them, stony (SDF) and muddy debris flow (MDF) are the two common types worldwide (Berti et al. 1999; Marchi et al. 2002; Mcardell et al. 2007; Tecca and Genevois 2009; Hu et al. 2011; Okano et al. 2012). The SDF (sometimes termed as coarse-grained debris flow or granular flow) was documented in some Dolomites areas of North-Eastern Italian Alps and at active volcanos of Japan (Marchi et al. 2002; Mcardell et al. 2007; Takahashi

2007; Tecca and Genevois 2009; Okano et al. 2012). This flow consists of relatively coarse sediments and muddy debris water such that the grain collision or friction plays an important role. The MDF commonly occurs in some mountain regions where the rocks are highly weathered and the soils are rich in clays and silts. This flow initiates either from numerous mass failures or runoff erosion as the watersheds have unlimited sediment supply (Bovis and Jakob 1999; Kang et al. 2004). Generally, MDF has fine, cohesive materials while SDF is coarse-grained and cohesionless (Wu et al. 1990; Coussot and Meunier 1996; Kang et al. 2006). Note that the two flows can block a river in some alpine regions. For example, three episodes of MDF from 4 to 12 July 2001 in Jiangjia Ravine, Yunnan Province, China delivered  $6.5 \times 10^5$  m<sup>3</sup> sediments and blocked Xiaojiang River (Wei et al. 2002). On 13-14 August 2010 and 11 July 2013, a clustering of depositional fans formed along the Min River, Sichuan province, China (Tang et al. 2011; Ge et al. 2015).

Debris flow deposits, as other deposits from giant landslides, rockslides, moraine dams, etc., play an important role in altering river profile and topography evolution (Korup 2006; Dang et al. 2009; Huang et al. 2012). These specified sites may remain a prolonged time and act the Knick-point. However, some of them may disappear owing to erosion and scouring of the fluvial process. At the confluence area, the debris flow dynamics and fan shape depend not on the dominant stress, but on the water flow. Chen and An (2007) and Dang et al. (2009) suggest that confluence angle, tributary slope, sediment concentration, discharge, and momentum are the main controlling factors influencing fan geometry. Some blockage types are concluded according to the ratio of momentum and discharge, deposits resilience stability index (He 2003; Dang et al. 2009; Stancanelli and Musumeci 2018). Some numerical simulation works examined the interaction between debris flows and water current (Chen and Peng 2006; Chen et al. 2011 and 2013). Recently, Stancanelli et al. (2015) reveal that the shape of the depositional fan is strongly influenced by the confluence angle, and the degree of an obstruction within the receiving channel is strongly influenced by the triggering scenario. By the particle diameter curves of debris in the tests of He (2003), Dang et al. (2009) and Stancanelli et al. (2015), the experimental debris flow belongs to either muddy or stony flows, while the difference in their depositional pattern is

few addressed. The interaction of SDF and MDF with water current is meaningful for the knowledge about debris flow dynamics and deposition features at the confluence area.

In this work, large-flume experiments were used to address the dynamics of SDF and MDF by the case of the orthogonal intersection. Particularly, this work mainly focuses on the differences of the depositional fan, which is affected by the water current drag and dominated stress. The damming ratio, depositional width in upstream and downstream and the dynamic scaling analysis were used to explore the differences in fan shapes. As some scholars examined the propagation phenomena of stony and muddy flow respectively, this work may provide some new inspirations about their risk assessment and their interactions with water current.

## 2 Debris Flow Damming River Events

After the Wenchuan earthquake, subsequent debris flows are more active and have higher magnitude than pre-quake events (Guo et al. 2016; Ma et al. 2017). Particularly, the catchments on both sides of Min River are susceptible to geological hazards as historical strong earthquakes, landslide, and debris flow dam breaching events were documented (Li et al. 2008; Zhao et al. 2019). Post-quake debris flows and river damming events were also documented in this area (Tang et al. 2011; Ma et al. 2013; Ge et al. 2015).

The rainstorms on 14 August 2010, 3 July 2011 and 10 July 2013 triggered clustering debris flows and some river damming events occurred (Tang et al. 2011; Ge et al. 2015). Fig. 1a shows the multiple fans on 14 August 2010. A total of 12 fans formed along the Min river section from Yingxiu to Yinxing town, Wenchuan city. Among them, the diverted water flow by no. 1 fan inundated the newly-constructed Yingxiu town (Fig. 1b). The no. 8 fan caused inundation of villages upstream (Fig. 1c). The no. 12 fan blocked the Min River, which raised the water level of upstream and resulted in inundation to the Yiwanshui village (Fig. 1d). Besides, debris flows in Gaojia gully blocked the Min River in the year 2010 and 2011 respectively. Such events were also documented in other areas. On 8 July 2001, a debris flow in Jiangjia Ravine blocked the Xiaojiang River (Wei et al. 2002). On 14 August 2010, debris flows in Xiaojia gully blocked the Yuzi

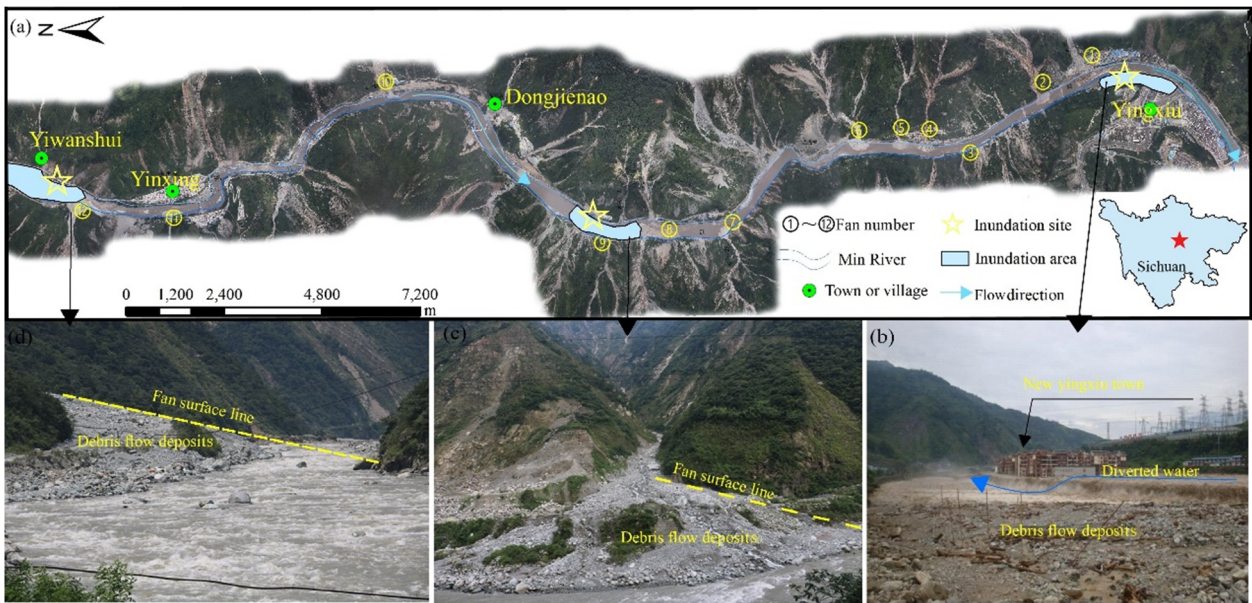


**Fig.1** Multiple depositional fans along the Min River section from Yingxiu town to Yinxing town in Sichuan province, China.

River, which is one of the tributaries of Min River (Chen et al. 2014). The debris flows in Jiangjia Ravine shares similar sediment component as the debris flows from Yingxiu to Yinxing town and in the Xiaojia gully (Fig. 2). The debris flow deposits of Gaojia in 2011 are coarser than those in the 2010 event. Besides, the debris flow deposits of Xiaojia gully in 2011 are coarser than the deposits in the 2010 event (Chen et al. 2014). In this work, the experimental debris was from the debris flow deposits in Gaojia gully. The particle diameter curves of experimental stony and muddy flows are similar to the debris flows of Gaojia gully in 2011 and other flows in 2010 respectively.

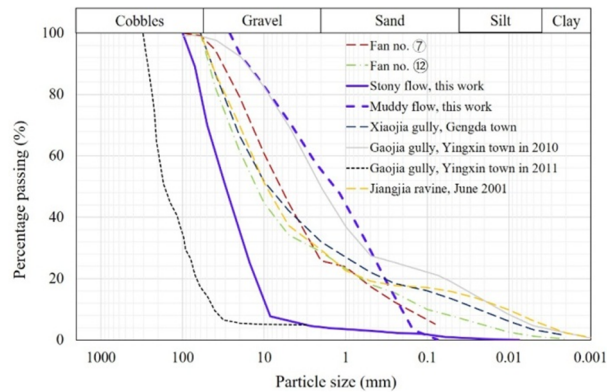


**Fig. 2** Particle diameter curve of debris flow deposit samplings in upstream of Min River and Jiangjia Ravine

### 3 Material and Methods

#### 3.1 Experimental set-up and procedure

Fig. 3 shows the current flume, debris flow flume and their installation. The current flume is 15 m long, 2 m wide and 1 m height, and consists of water current flume, water tank, and sand tank. The water flow in each test is recirculated by the connection between the water tank and the sand tank. The pump in the water tank continuously supplies water to the current flume. The debris flow flume is 6 m long, 0.33 m width and 0.4 m height, and is 5 m to the water incoming.

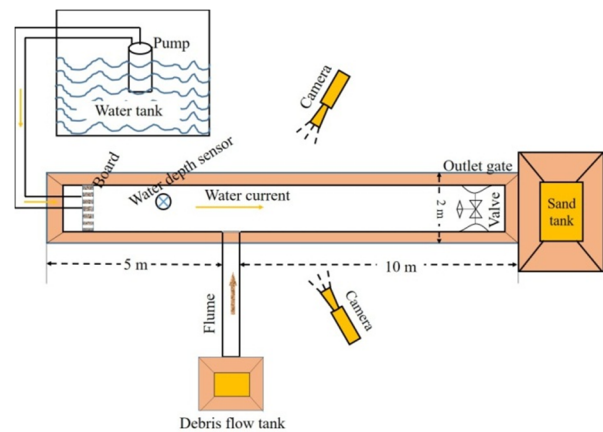


**Fig. 3** Graph showing the experimental flume.

A press sensor records the water level ( $H_w$ , m). Besides, two cameras on both sides record the velocity

of the water current and debris flow. The debris flow flume slope is adjustable between  $10^\circ$  and  $20^\circ$ , which



covers the channel gradient of watersheds with debris flow events in the year of 2010. The junction angle of the current flume and debris flow flume is fixed at 90° because the majority of watershed outlet orthogonally connects to Min River, as exemplified by Fig. 1.

### 3.2 Dimension and dimensionless numbers

#### 3.2.1 Dimension numbers

The water flow velocity ( $U_w$ , m/s) in the current flume was calculated by the time difference of plastic foam passage between two sections. The travel time at a distance of 0.4 m determines the debris flow velocity ( $U_d$ , m/s). The flow depth ( $H_d$ , m) was recorded by the flow marks on both flume sidewalls. The fan shape and water level in each test are possibly different because debris flow may have varied momentum. Therefore, the shape and thickness of the depositional fan were measured by a steel net with many probes of 0.1 m interval. As the water level in upstream differentiates due to depositional fan, the relative water level is used here, which is calculated by the measured water level minus initial water level.

The ratio of depositional width in upstream and downstream express the diversion ratio (e.g.,  $D_u/D_d$ , where  $D_u$  is the upstream width,  $D_d$  is the downstream width). The runout distance across the current flume defines as  $R_l$ , which is calculated along the central line of debris flow flume (Fig. 4). As the debris flow damming river has a close relationship with velocity and unit weight of debris flow, the ratio between the momentum of debris flow and water current ( $0.33\rho_d U_d H_d / 2\rho_w H_w U_w$ ), damming ratio ( $R_l/2$ ), and

diversion ratio ( $D_u/D_d$ ) were combined to analyze the interaction and fan shape.

#### 3.2.2 Dimensionless numbers and analysis

The experiment in this work mainly elucidates the interaction of debris flow and water current at the confluence area. The small size of the apparatus typically limits the scaling problems. Therefore, the contribution of this work is of the utmost importance if dynamic similarities are attained. During debris flow movement, the inertial forces arise from collisions between solid grains, viscous shear forces are controlled by pore fluid viscosity, and frictional forces are associated with long-lasting contacts between grains, the pore pressures buffering the inertial and frictional forces are associated with inertial fluid velocity fluctuations. Their relative importance is described by four dimensionless numbers,  $N_{Bag}$ ,  $N_{Sav}$ ,  $N_{Fric}$ , and  $N_{Rey}$ , which is evaluated in this work and compared with other natural or experimental debris flows (Iverson and Denlinger 2001; Iverson 1997; Lanzoni et al. 2017).

The Savage number,  $N_{Sav}$ , defines the ratio of inertial to frictional stresses:

$$N_{Sav} = \frac{\rho_s \gamma^2 \delta^2}{(\rho_s - \rho_f) g h \tan \phi} \quad (1)$$

where  $\rho_s$  and  $\rho_f$  are the density of grains and fluid phase within debris flows ( $\text{kg}/\text{m}^3$ );  $g$  is gravity acceleration ( $9.8, \text{m}/\text{s}^2$ );  $\delta$  is the mean diameter of the solid particles ( $D_{50}$ , mm);  $\phi$  is internal friction angle ( $^\circ$ ),  $h$  is flow depth (m),  $\gamma$  is the shearing rate (e.g.,  $U_d/H_d$ ).

The Bagnold number,  $N_{Bag}$ , measures the ratio of

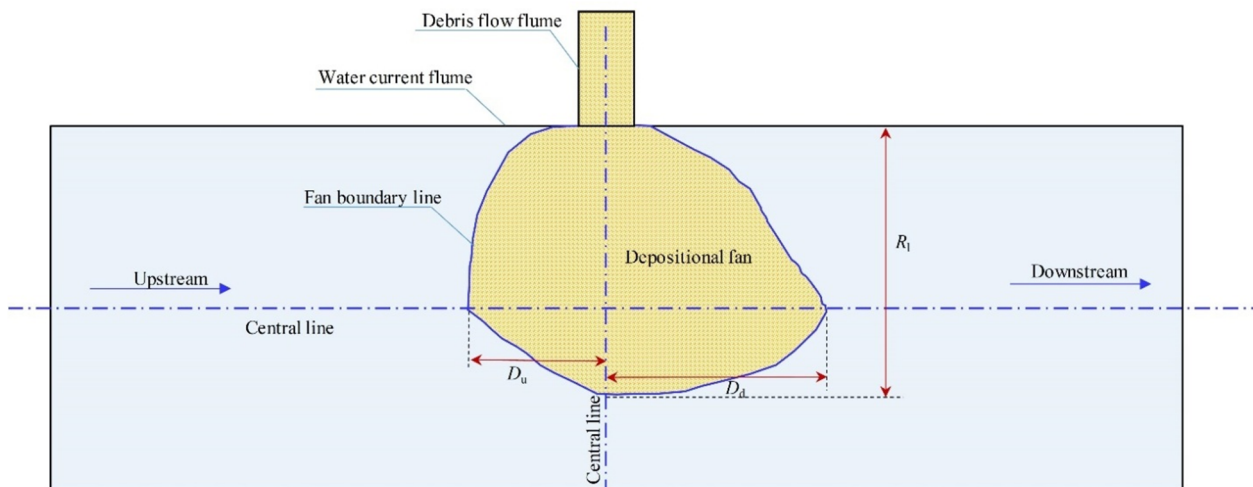


Fig. 4 Simplified graph showing the geometrical parameters of depositional fan at the confluence area



inertial grain collision to viscous stresses:

$$N_{Bag} = \frac{v_s \rho_s \gamma \delta^2}{1-v_s \mu} \tag{2}$$

where  $v_s$  is the solid phase volume fraction;  $\mu$  is the dynamic viscosity of interstitial fluid (Pa·s).

The Reynold number,  $N_{Rey}$ , measures the ratio of inertial fluid velocity fluctuations to viscous stresses, and is in the form:

$$N_{Rey} = \frac{\rho_f \gamma \delta^2}{\mu} \tag{3}$$

The Friction number,  $N_{Fric}$ , measures the ratio of grain contact friction to viscous shear:

$$N_{Fric} = \frac{v_s (\rho_s - \rho_f) g h \tan \phi}{1-v_s \gamma \mu} \tag{4}$$

In general, the collisional regime prevails in some natural or laboratory-generated debris flows if the  $N_{Sav} > 0.1$  and  $N_{Bag} > 450$  (Lanzoni et al. 2017). Otherwise, the frictional regime or the viscous shear dominate. The friction regime and inertial fluid velocity will dominate over viscous shear in some debris flow if the  $N_{Fric} > 2000$  and  $N_{Rey} > 1$ , respectively (Iverson 1997).

## 4 Results

Several pre-experiments checked the runout distance of the debris flows. We found that the

experimental SDF commonly traveled at a faster speed than MDF, no matter what the debris flow volume is. Then, a total of 7 SDF and 11 MDF tests were carried out (Table 1). The bulk densities of debris flows were  $> 1.9 \text{ g/cm}^3$ . The bulk densities of MDF were commonly higher than SDF, owing to the higher fine fraction. The slope gradient of debris flow flume in SDF tests was between  $14^\circ$  and  $16.5^\circ$ . The debris flow velocities commonly exceeded  $1.0 \text{ m/s}$  and flow depths were less than  $0.2 \text{ m}$ . In the 11 MDF tests, the slope gradient was  $10^\circ$ , the flow depths were  $> 0.2 \text{ m}$  and the debris flow velocities were in the range of  $0.41$  and  $0.67 \text{ m/s}$ . As a relatively lower velocity than SDF, the runout distance of MDF ranges from  $1.00$  to  $2.00 \text{ m}$ .

### 4.1 Deposition phase of debris flows at the confluence area

#### 4.1.1 Fan geometry differences

The depositional fans of SDF have a length exceeding  $2.0 \text{ m}$  because the velocity ranges from  $1.59$  to  $2.32 \text{ m/s}$  (Table 1), and the width of the current flume is limited. Because the depositional fans are completely buried in water, the water current does not divert, and the water flows over the fan surface. Furthermore, the SDF depositional fans are long-rectangle shape (Fig. 5, and Fig. 6a and 6c).

**Table 1** Dimensional parameters in 18 tests.

DF	No	$\rho_d$ (kg/m <sup>3</sup> )	$H_d$ (m)	$U_d$ (m·s <sup>-1</sup> )	$\theta$ (°)	$V$ (m <sup>3</sup> )	$H_w$ (cm)	$U_w$ (cm·s <sup>-1</sup> )	$R_l$ (cm)	$Du/Dd$
SDF	1	1960	0.16	2.28	15.6	0.554	11.5	30.0	200	0.54
	2	2130	0.18	2.32	15.6	0.691	8.5	24.0	200	0.79
	3	2110	0.18	2.10	15.6	0.691	19.5	43.0	200	0.49
	4	2190	0.17	1.81	16.5	0.554	19.5	45.0	200	0.54
	5	2190	0.19	2.68	14.0	0.590	20.0	48.0	200	0.42
	6	2100	0.17	1.59	14.0	0.410	20.0	48.0	200	0.35
	7	2070	0.14	1.90	14.0	0.288	19.0	38.7	200	0.52
MDF	1	2230	0.27	0.45	10.0	0.569	19.5	45.0	100	0.79
	2	2200	0.34	0.67	10.0	0.596	19.5	67.0	100	0.87
	3	2150	0.18	0.41	10.0	0.616	19.5	41.0	200	0.30
	4	2100	0.30	0.60	10.0	0.518	21.0	60.0	200	0.34
	5	2200	0.30	0.55	10.0	0.548	20.0	55.0	200	0.33
	6	2250	0.29	0.60	10.0	0.720	19.5	60.0	110	0.59
	7	2250	0.32	0.55	10.0	0.864	19.5	55.0	130	0.59
	8	2250	0.16	0.60	10.0	0.950	24.0	60.0	130	0.63
	9	2250	0.25	0.60	10.0	1.037	25.0	60.0	140	0.37
	10	2250	0.48	0.60	10.0	1.253	25.0	60.0	160	0.37
	11	2300	0.54	0.56	10.0	1.411	26.0	60.0	184	0.60

**Note:** Stony (SDF) and muddy debris flow (MDF);  $\rho_d$ ,  $H_d$  and  $U_d$  are the bulk density, flow depth and velocity of debris flow,  $\theta$  is the slope gradient of debris flow flume,  $V$  is the total debris flow volume,  $H_w$  and  $U_w$  are the flow depth and velocity of water flow,  $R_l$  is runout distance of debris flow and is calculated along the central line of debris flow flume,  $Du$  and  $Dd$  are the distance from the central line of debris flow flume to the upstream and downstream distal point of depositional fan.

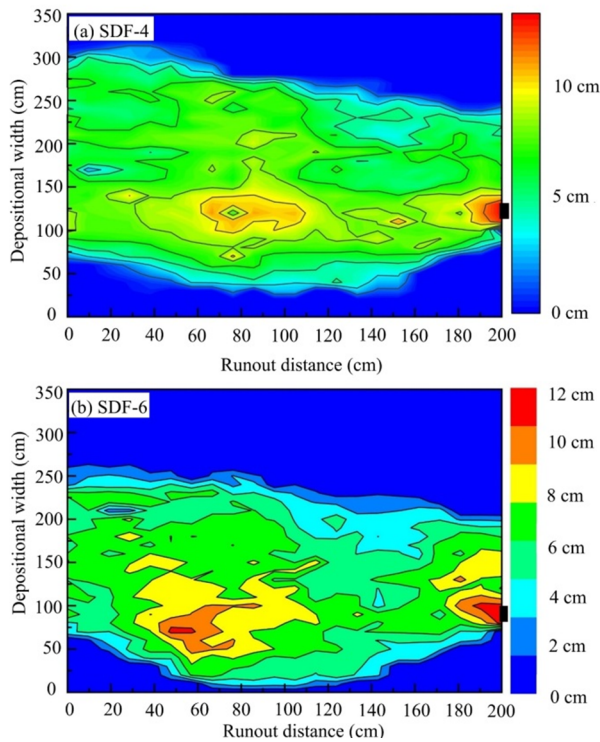


**Fig. 5** Color graphs showing the depositional depth at the confluence area: (a) depositional depth in stony debris flow test no. SDF-4; (b) depositional depth in stony debris flow test no. SDF-6; the black rectangle represents the location of debris flow flume outlet.

The slope gradients of debris flow flume in MDF tests are milder than SDF. The velocity ranges from 0.45 to 0.67 m/s, and the flow depth is between 0.18 and 0.26 m. Their runout distance ranges from 1.0 to 2.0 m, indicating that the MDFs partially or completely block the water current flume. Fig. 7 shows the depositional fan in tests no. MDF - 2, 8, 10 and 5. Corresponding runout distances are 1.00, 1.30, 1.94 and 2.00 m, respectively. In tests with runout distance < 2.00 m, debris flow can form a fan shape by the case of MDF - 2, 8 and 10, as shown in fig. 6a, 6b, and 6c. In tests with runout distance  $\geq$  2.00 m, the fan surface is eroded by the water current and the erosion extent increase as the distance to debris flow flume outlet (Fig. 7d). As the MDFs have high fine fractions and travel slowly, the fan surface for tests with runout distance  $\geq$  2.00 m is not as rugged as the SDF (Fig. 6e). For the tests with runout distance < 2.00 m, the depositional fan diverted the water current, promoting the water velocity near and at the narrow section. Therefore, the fines within MDF fan in upstream were delivered a lot while the downstream fan suffers light erosion from water (Fig. 6d, 6f-6h).

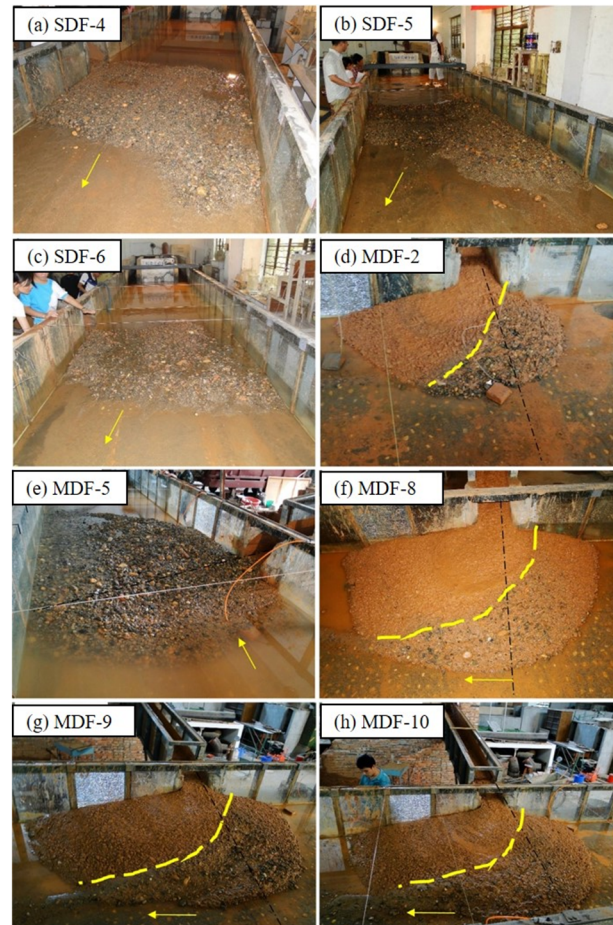


**Fig. 6** The surface features of the depositional fan of SDF (stony debris flow) and MDF (muddy debris flow): (a, b and c) downstream view of depositional fans in tests SDF -4, -5, and -6; (d) frontal view of depositional fan in test MDF-4; (e) upstream view of depositional fan in test MDF-5; (f, g and h) frontal view of depositional fans in tests MDF-8, -9 and -10. The yellow arrow indicates the water current direction, dot-yellow line marks the boundary of fan with and without water scouring.

#### 4.1.2 Relative water level

Depositional fan may result in inundation and dam breaching, which is closely related to damming pattern, the fan height and sediment component (Cui et al. 2009; Chen et al. 2011). In general, the upstream inundation risk from complete damming is highest. In evaluating the potential risk, the risk of upstream inundation commonly bases on the relative water level (Cui et al. 2013b; Zou et al. 2018), which is calculated by the water flow level before and after debris flow block river. However, such inundation risk may differentiate for SDF and MDF, according to the fan shapes shown in Figs. 5, 6 and 7.

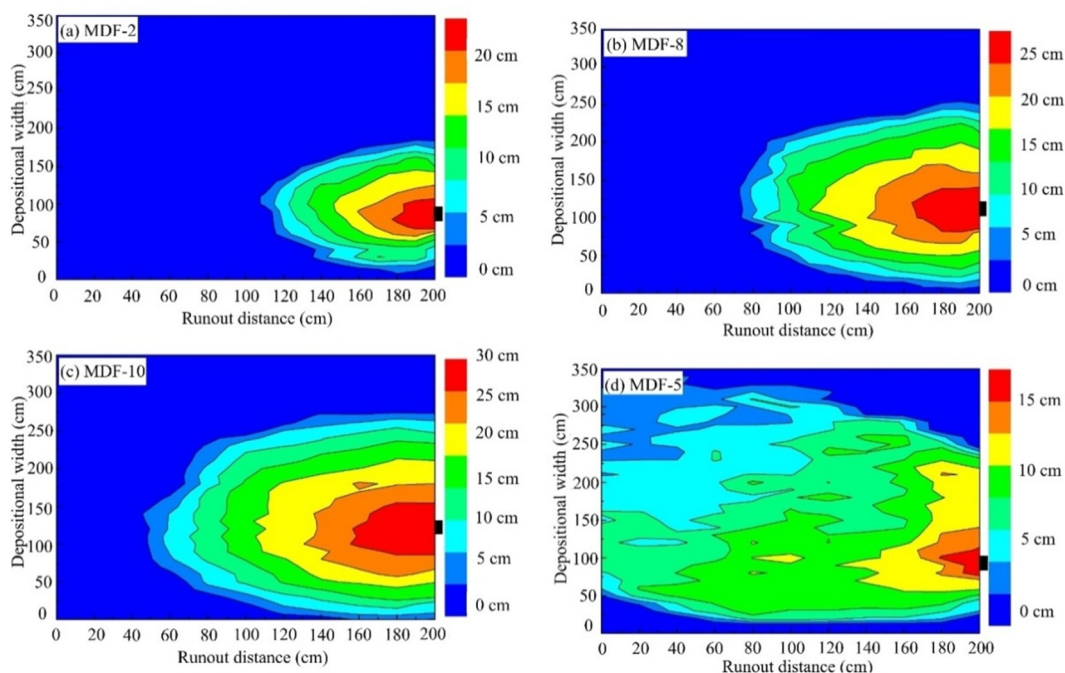


**Fig. 7** Color graphs showing the depositional fan in muddy flow tests no. MDF-2(a), MDF-8(b), MDF-10(c) and MDF-5(d); the black rectangle represents the location of debris flow flume outlet.

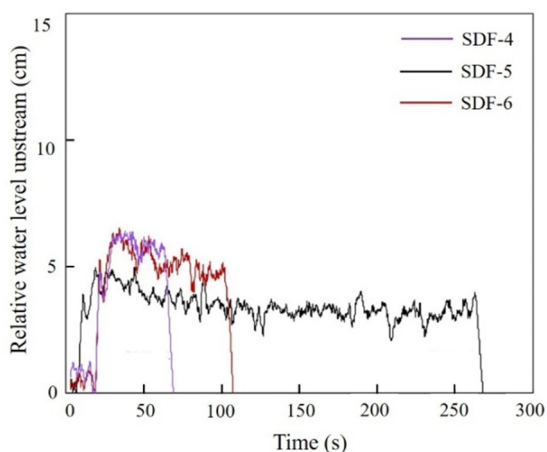


**Fig. 8** The upstream relative water level in stony debris flow tests no. SDF -4, -5 and -6.

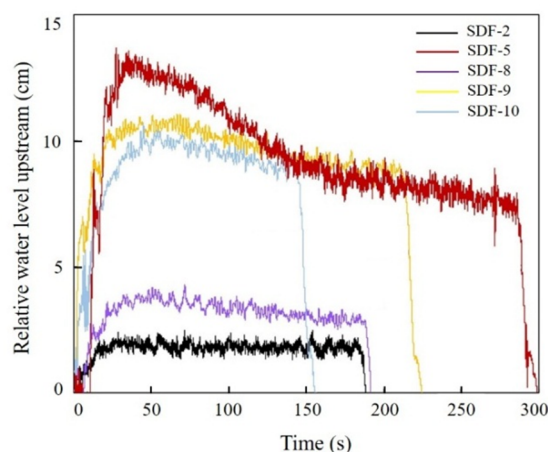


**Fig. 9** The upstream relative water level in muddy debris flow tests no. MDF-2, -5, -8, -9 and -10

The relative water levels in tests of SDF and MDF are shown in Figs. 8 and 9, respectively. Based on the peak level of three curves of SDF and the two curves of MDF – 2 and 8, the risk from MDF with damming ratios of 0.5 and 0.65 seems to be similar to the three SDF with damming ratio of 1.0. The relative water level is 14%, 14%, 10%, 4% and 8% of the initial water level in the three SDF tests and two MDF tests. The debris volume of SDF - 4, 5, 6 is smaller than MDF -2 and 8. This implies that the upstream inundation from SDF is still higher. Furthermore, Fig. 8 shows the relative water level for MDF – 2, 8, 9, 10 and 5.

Correspondingly, and dam ratios are 0.5, 0.65, 0.7, 0.8 and 1, respectively. In detail, the relative water levels are 18%, 18% and 25% of initial water level for MDF - 8, 9 and 5. The percentage of relative water level to the initial water level positively increases with the damming ratio for MDF. Therefore, the upstream inundation risk for MDF positively relates to the runout distance in the main river. In comparison, the risk of upstream inundation from MDF is higher than SDF, if they have a similar volume to completely block a river.



### 4.1.3 Momentum ratio, damming ratio and diversion effect

In general, the criteria of river damming mainly depends on the momentum ratio and deposited volume (Chen and An 2007; Dang et al. 2009). If the debris flows exhibit high momentum over the water current, the damming potential greatly increases (He 2003). The damming ratio is commonly represented as the runout distance to the river width (Du et al. 2014), while no documents address the diversion ratio (e.g.,  $D_u/D_d$ ). In some tests of this work, the incoming debris flow occupy entire width of water current flume, the runout distance is mainly constrained by the channel width. Therefore, the tests with damming ratio of 1 are not for analysis when addressing damming ratio with momentum ratio and diversion ratio.

In the 7 SDF tests, the minimum momentum ratio is 0.95. All SDF completely block water current, which may attribute to limited current flume width and high velocity. Some MDFs completely block water current flume and have a momentum far less than the water current, as exemplified by the tests MDF- 3, 4 and 5 (Table 1). Fig. 10 shows the relationship between momentum ratio with diversion and damming ratio. It seems that the diversion ratio decrease as increasing momentum ratio, indicating that the depositional fan mainly spread downstream. Besides, the 8 dataset of MDF indicates that damming ratio increase as the momentum ratio.

The damming and diversion ratios of MDF, together with the 12 debris flow fans along the Min River, are plotted in Fig. 1. The empirical line in Fig. 11 was derived by fitting the data of experimental MDF and the 12 debris flow fans. This line illustrates that the diversion ratio decreases as the damming ratio increase. Assuming that the damming ratio is zero, the depositional widths in upstream and downstream are roughly equivalent. This relationship implies that MDF with shorter runout distance weakly interacts with the water current. Additionally, the runout distances of the 12 debris flow fans were underestimated, because the marginal area of the fan was eroded. Fig. 11 also presents the damming ratio and diversion ratio of the three debris flows no. 1, 8 and 12 in Fig. 1. The three debris flows caused severe damage as they either raised the water level or diverted the water path to the other side. Considering the water erosion on the marginal area of the deposited fan, the three debris flows should have

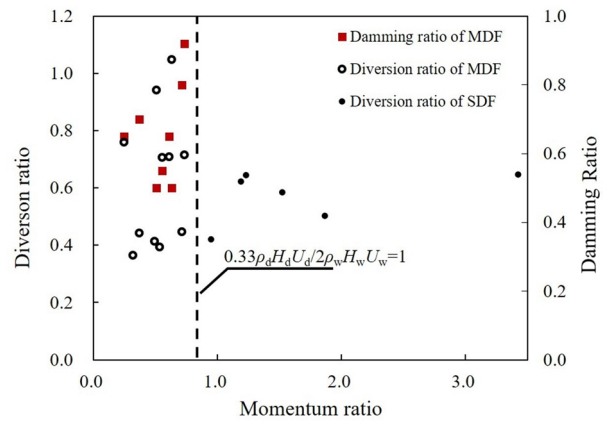


Fig. 10 The momentum ratio, diversion ratio and damming ratio in tests.

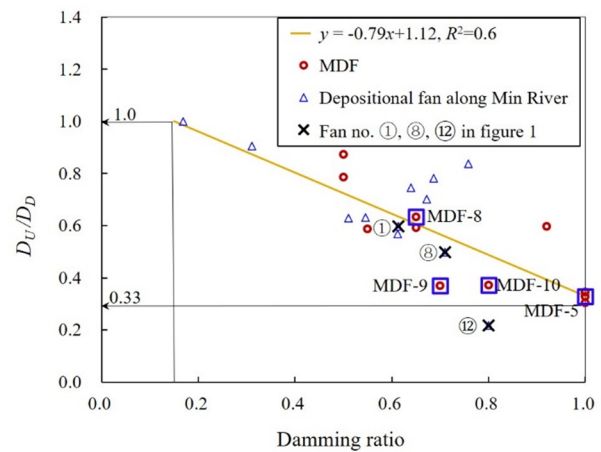


Fig. 11 The relationship between damming ratio and diversion ratio of SDF (stony debris flow) and MDF (muddy debris flow).

damming ratio over 0.8 and their diversion ratios are 0.6, 0.5 and 0.21 respectively, which is the smallest among the 12 fans.

### 4.2 Dimensionless analysis of experimental debris flow

Experimental or natural debris flows are usually dominated by stress regime between inertial and friction (Iverson 1997; Zhou and Ng 2010). Some of them tend to be friction dominated if fine fractions are relatively abundant and sediment concentration exceeds 0.5 (Campbell 1990; Takahashi 2007). In this work, both of SDF and MDF have solid fraction exceeding 0.5 while the solid fractions of MDF are higher. In evaluating the debris flow physics, Fig. 12 shows the  $N_{Sav}$ ,  $N_{Rey}$ ,  $N_{Fric}$ , and  $N_{Bag}$  of experimental flows, debris flows in Jiangjia Ravine and Kamikamihorizawa (Kang et al. 2006; Zhou and Ng

**Table 2** Data of dimension and dimensionless numbers in tests and other cases.

No	Cases	$H_d$ (m)	$\rho_s$ (kg cm <sup>-3</sup> )	$\rho_f$ (kg cm <sup>-3</sup> )	$v_s$	$D$ (m)	$U_d/H_d$ (s <sup>-1</sup> )	$\theta$ (°)	$\mu$ (Pa s)	$N_{Sav}$	$N_{Bag}$ (×10 <sup>4</sup> )	Resources /Reference
1	Yake Dake	2.00	2600	1200	0.60	0.0200	3.00	9.0	0.100	0.0340	1.360	Takahashi (2007)
2	Kamikami- Horizawa	2.00	2600	1200	0.60	0.0200	3.00	15.0	0.100	0.0340	0.468	Takahashi (2014); Iverson and Denlinger (2001)
3	USGS Flume	0.10	2700	1100	0.60	0.0010	100.00	31.0	0.001	0.200	0.040	Iverson (1997)
4	Acquabona watershed	2.00	2650	1200	0.60	0.2000	4.00	16.0	0.100	0.060	1.850	Berti (1999, 2000)
5	Large USGS flume	0.20	2700	1000	0.60	0.0100	100.00	31.0	0.010	0.203	0.203	Iverson and Vallance (2001)
6	Small USGS flume	0.04	2650	1000	0.50	0.0060	50.00	18.0	0.001	0.133	0.286	Parsons et al (2001)
7	Straight Chute Flume	0.06	2650	1100	0.60	0.0001	10.00	13.0	0.500	2.910×10 <sup>-6</sup>	7.950×10 <sup>-8</sup>	Parsons et al (2001)
8	Drum Experiment I	0.05	2650	1000	0.55	0.0100	20.00	10.0	2×10 <sup>-5</sup>	0.0817	32.400	Hsu et al (2008)
9	Drum Experiment II	0.05	2650	1000	0.55	0.0100	10.00	10.0	0.001	0.0328	3.240	Stancanelli et al (2015)
10	Stony debris flow	0.05	2650	1000	0.43	0.00300	20.00	17.0	0.001	0.012	0.114	Zhou and Ng (2010)
11	Surge flows	-	2750	-	0.60	0.0050	-	-	0.500	<0.010	-	Zhou and Ng (2010)
12	Continuous flows	-	2750	-	0.45	0.0050	-	-	0.500	<0.010	-	Zhou and Ng (2010)
13	SDF	0.17	2650	1127	0.58 -0.72	0.3000	12.67	14 -15.6	0.090	0.173	0.717	This work
14	MDF	0.31	2650	2008	0.67 -0.79	0.0014	2.01	10.0	0.440	1.790×10 <sup>-5</sup>	8.510×10 <sup>-7</sup>	This work

**Note:**  $H_d$ ,  $\rho_s$ , and  $\rho_f$  are the flow depth, density of grains and fluid phase within debris flows;  $v_s$  is the solid phase volume fraction;  $d$  is the particle diameter;  $U_d$  is the mean debris flow velocity;  $\theta$  is the slope gradient of experimental flume or natural debris flow channel;  $\mu$  is the dynamic viscosity of interstitial fluid;  $N_{Sav}$  and  $N_{Bag}$  are the Savage and Bagnold number. SDF, stony debris water; MDF, muddy debris flow.

2010; Okano et al. 2012). Besides, Table 2 lists some documents addressing the  $N_{Sav}$  and  $N_{Bag}$  of natural or experimental debris flows.

Though the normal stress ( $\rho g h \cos \theta$ ) of experimental SDF is no less than the stony flows in Kamikamihorizawa, their  $N_{Sav}$  and  $N_{Bag}$  are similar (Fig. 12a and 12b). All  $N_{Sav}$  of experimental SDF exceed 0.1 and most  $N_{Sav}$  of stony flows in Kamikamihorizawa exceed 0.1 (Fig. 12a). Additionally, the  $N_{Sav}$  for the debris flows in the Acquabona watershed, Italy ranges from 0.02 to 0.93 and 0.06 on average (Berti et al. 1999, 2000; Table 2). The  $N_{Sav}$  for the debris flows in Chalk cliffs, Houenshan, Moscardo are 0.19, 0.05, 0.001-0.004 and 0.01-1.96 respectively (Lanzoni et al. 2017). The debris flows in USGS flume exhibit collision dominance as the  $N_{Sav}$  exceeds 0.1 and is close to the experimental SDF. Though the  $N_{Sav}$  and  $N_{Bag}$  of these debris flows differ greatly, most of their magnitude is in same range, and their values of SDF in this work can be comparable to some natural events.

The surge flows and continuous flows in Jiangjia Ravine commonly have  $N_{Sav} < 0.01$  (Zhou and Ng 2010). The experimental MDF and flows in Straight Chute Flume have the smallest  $N_{Sav}$  among the debris flows in Table 2. The  $N_{Bag}$  of experimental SDF and stony flows in Kamikamihorizawa is far more than the MDF and exceeds 200 (fig. 12b) and even 450. This illustrates that they may be in a fully inertial regime. Besides, the debris flows in USGS flume exhibit collision dominance as the  $N_{Sav}$  exceeds 0.1 and is

close to the experimental SDF. Lanzoni et al. (2017) also pointed out that the dynamics of coarse-grained debris flow were governed by particle collision. The  $N_{Bag}$  for debris flows in Table 2 implies that the majority of them are collision-dominated while this stress in the experimental MDF and Straight Chute Flume are negligible.

Unlike the collision stress dominates stony flow, the turbulent mixing stresses and viscosity are of utmost importance to the muddy flow and viscous flow. The larger  $N_{Rey}$  represents that the turbulent mixing stress dominates flow movement. In Fig. 12c, the experimental SDF and stony flows in Kamikamihorizawa share similar  $N_{Rey}$ , followed by a decreasing sequence of the surge flow, continuous flow and the experimental MDF. Besides, Lanzoni et al. (2017) analyzed the  $N_{Rey}$  of some natural and experimental flows, and found that these dimensionless numbers commonly are in the same range with the experimental SDF and far larger than the MDF. This indicates that particle collision can generate strong turbulent effect during stony movement, which causes high pore water pressure supporting long traveling of debris flows. In Fig. 12d, the  $N_{Fric}$  of experimental MDF is different from the experimental SDF and the stony flows in Kamikamihorizawa, while is similar to the surge flow and continuous flow. This indicates that the viscous shear stress tends to exceed friction stress for the experimental MDF.

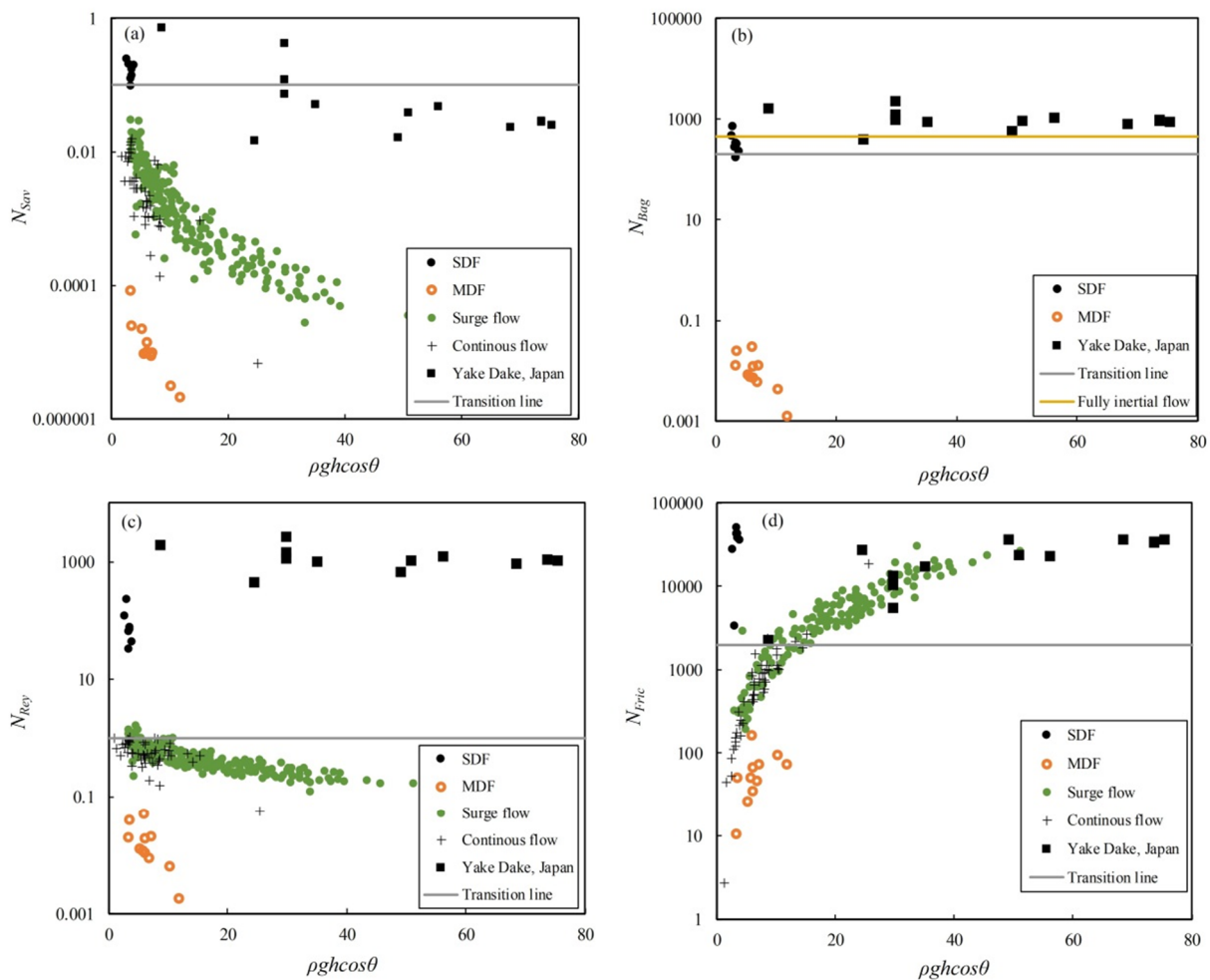


**Fig. 12** Comparison of dimensionless numbers describing debris flow movement of SDF and MDF: (a)  $N_{sav}$ ; (b)  $N_{Bag}$ ; (c)  $N_{Rey}$ ; (d)  $N_{Fric}$ . Besides, some data of surge flows and continuous flows in Jiangjia Ravine, China and the debris flows in Kanikamihorizawa, Mountain Yakedake, Japan are also plotted together for comparison.

### 5 Discussions

As known to all, Takahashi (2007) classified debris flows into three types, including stony type, turbulent-muddy type, and viscous type. The three flows are mainly dominated by grain collision stress (larger  $N_{Bag}$ ), turbulent mixing stress (high  $N_{Rey}$ ) and viscous stress (small  $N_{Bag}$  and  $N_{Rey}$ ) respectively. The dimensionless analysis illustrates that the stony flows in this work are dominated by particle collision and inertial fluid velocity fluctuates heavily. Particularly, the values of  $N_{sav}$  and  $N_{Bag}$  are comparable to some natural stony flows. For the muddy flows in this work, the dimensionless analysis proves that this flow is dominated by viscous shear stress and the inertial fluid velocity fluctuation does not fluctuate so heavily as the stony flow. The reason why the  $N_{sav}$ ,  $N_{Rey}$  and

$N_{Fric}$  of experimental MDF are smaller than the debris flow in Jiangjia Ravine lies in that the sediment component are finer while the sediment component of debris flow in Jiangjia Ravine have coarse grains. As the rheology and dominated stress of stony and muddy flows are completely different, the depositional fan shape can be distinctive.

The fan shape at the confluence area does not depend on the rheology or dominated stress (Coussot and Meunier 1996), but also on the interaction with the current (Stancanelli et al. 2015; Lanzoni et al. 2017). The SDF propagates quickly, exhibits strong particle collision and inertial fluid velocity fluctuation, and has large void between coarse grains. The MDF moves slower than SDF, has weak particle collision, slight inertial fluid velocity fluctuation and small void. These factors together result in the differences in the depositional fans. Furthermore, the experiment results and the 12 depositional fans along the Min



River from Yingxiu to Yinxing town together reveal that the diversion ratio of the MDF depositional fan decrease as the damming ratio increase. The comparison present that relative water level is mainly controlled by damming ratio for MDF, while the diversion ratio may be the other factor for SDF. Therefore, the upstream inundation risk from complete damming by MDF is higher than SDF.

Presently, most of the depositional fans along the Min River (e.g., river section from Yingxiu to Yinxing town) disappeared as times elapsed. This illustrates that these deposits are mainly composed of fine sediments. However, some authors proved that subsequent debris flows in some watersheds near the epicenter of Wenchuan earthquake will become coarse as fine sediments are missing (Chen et al. 2014). Besides, the runout distance of debris flows will decrease as times elapsed to the first debris flow event (Zhang et al. 2013). Though the inundation risk of stony flows seems to be not comparable to muddy flows, such flows have stronger impact force and erosion ability. Therefore, the high possibility of stony flows exists in subsequent years, while the inundation risk may decrease.

## 6 Conclusions

The interaction between depositional fan of debris flow and the current at the confluence area of mountainous river closely relates to the river topography and the inundation risk. In this work, the propagation of stony and muddy debris flow in the case of the orthogonal intersection with water current were examined by a total of 18 large flume tests and analyzed on basis of the differences in depositional fan shapes, damming ratio, diversion ratio and dimensionless numbers. Following results can be drawn:

(1) The experimental stony flows commonly form a depositional fan with long rectangle shape even

though they have a momentum nearly equivalent to the water current. The muddy flows generally form a fan-shaped depositional area and tend to block a river even they have a smaller momentum than water current. The diversion ratio of depositional fan by muddy flows at the confluence area increases with the damming ratio.

(2) Comparison of the relative water level upstream indicate that the risk of damming river from muddy flows is higher than stony flows assuming that they have a similar volume and the damming ratio is 1.0.

(3) The values of dimensionless numbers reveal that experimental stony flows were dominated by grain collision stress combined with turbulent mixing stress, while the muddy flows were dominated by viscous shear stress over friction stress respectively. This indicates that stony flows will strongly interact with the water current while the muddy flows will not, which can be used to explain the differences in depositional fan shapes in the experiments.

## Acknowledgements

The author sincerely thanks the comments from two anonymous reviewers. This research was funded by the National Key Research and Development Program of China (2017YFC0505602), Second Tibetan Plateau Scientific Expedition and Research Program (Grant No. 2019QZKK0902) and the National Natural Science Foundation of China (No. 41601004), and in part by Applied Basic Research Project of Sichuan Province (No. 2018JY0169), Scientific and Technological Project in Henan Province (212102310055). The experiments were carried out during the author's four years of Ph. D study in Southwest Jiaotong University and the teamwork members joining in the experiments are highly appreciated.

## References

- Berti M, Genevois R, Simoni A, et al. (1999) Field observations of a debris flow event in the Dolomites. *Geomorphology* 29: 256–274.  
[https://doi.org/10.1016/S0169-555X\(99\)00018-5](https://doi.org/10.1016/S0169-555X(99)00018-5)
- Bovis MJ, Jakob M (1999) The role of debris supply conditions in predicting debris flow activity. *Earth Surf Process Landf* 24(11): 1039–1054.

- [https://doi.org/10.1002/\(SICI\)1096-9837\(199910\)24:11<1039::AID-ESP29>3.0.CO;2-U](https://doi.org/10.1002/(SICI)1096-9837(199910)24:11<1039::AID-ESP29>3.0.CO;2-U)
- Berti M, Genevois R, LaHusen R, et al. (2000) Debris flow monitoring in the acquabona watershed on the Dolomites (Italian alps). *Phys Chem Earth Part B: Hydrol Oceans Atmos* 25(9): 707–715.  
[https://doi.org/10.1016/S1464-1909\(00\)00090-3](https://doi.org/10.1016/S1464-1909(00)00090-3)

- Braun A, Cuomo S, Petrosino S, et al. (2018) Numerical SPH analysis of debris flow run-out and related river damming scenarios for a local case study in SW China. *Landslides* 15(3): 535-550.  
<https://doi.org/10.1007/s10346-017-0885-9>
- Campbell CS (1990) Rapid granular flows. *Annu Rev* 22: 57-92.  
<https://doi.org/10.1146/annurev.fl.22.010190.000421>
- Coussot P, Meunier M (1996) Recognition, classification and mechanical description of debris flows. *Earth-Sci Rev* 40(3-4):209-227.  
[https://doi.org/10.1016/0012-8252\(95\)00065-8](https://doi.org/10.1016/0012-8252(95)00065-8)
- Cui P, Chen XQ, Wang YY, et al. (2005) Jiangjia Ravine debris flows in south-western China. In: *Debris-flow Hazards and Related Phenomena*. Springer Praxis Books. Springer, Berlin, Heidelberg.  
[https://doi.org/10.1007/3-540-27129-5\\_22](https://doi.org/10.1007/3-540-27129-5_22)
- Cui P, Han YS, Chen XQ (2009) Distribution and risk analysis of dammed lakes reduced by Wenchuan earthquake. *J Sichuan Univ (Eng Sci Ed)* 41: 35-42 (In Chinese).  
<https://doi.org/10.15961/j.jsuese.2009.03.024>
- Chen SC, Peng SH (2006) Two-dimensional numerical model of two-layer shallow water equations for confluence simulation. *Adv Water Resour* 29(11): 1608-1617.  
<https://doi.org/10.1016/j.advwatres.2005.12.001>
- Chen SC, An S (2007) Flume experiment of debris flow confluence formed alluvial fan in the main channel, in River, Coastal and Estuarine Morphodynamics: RCEM 2007, edited by Dohmen-Janssen CM, Hulscher SJMH. Taylorand Francis, London, U. K. pp. 829-835.  
<https://doi.org/10.1201/9780429064029>
- Chen RD, Liu XN, Cao SY, et al. (2011) Numerical simulation of deposit in confluence zone of debris flow and mainstream. *Sci China-Technol Sci* 54(10): 2618-2628.  
<https://doi.org/10.1007/s11431-011-4510-1>
- Chen XQ, Cui P, Li Y, et al. (2011) Emergency response to the Tangjiashan landslide-dammed lake resulting from the 2008 Wenchuan earthquake. *Landslides* 8:91-98.  
<https://doi.org/10.1007/s10346-010-0236-6>
- Chen RD, Liu XN, Huang E, et al. (2013) Numerical analysis of emergency river restoration scheme for Qingping mega debris flow. *J Mt Sci* 10(1): 130-136.  
<https://doi.org/10.1007/s11629-013-2120-z>
- Cui P, Zhou GGD, Zhu XH, et al. (2013a) Scale amplification of natural debris flows caused by cascading landslide dam failures. *Geomorphology* 182:173-189.  
<https://doi.org/10.1016/j.geomorph.2012.11.009>
- Cui P, Zou Q, Xiang LZ, et al. (2013b) Risk assessment of simultaneous debris flows in mountain townships. *Prog Phys Geogr* 37(4): 516-542.  
<https://doi.org/10.1177/0309133313491445>
- Chen HX, Zhang LM, Zhang S (2014) Evolution of debris flow properties and physical interactions in debris-flow mixtures in the Wenchuan earthquake zone. *Eng Geol* 182:136-147.  
<https://doi.org/10.1016/j.enggeo.2014.08.004>
- Dang C, Cui P, Cheng ZL (2009) The formation and failure of debris flow-dams, background, key factors and model tests: Case studies from China. *Environ Geol* 57: 1901-1910.  
<https://doi.org/10.1007/s00254-008-1479-6>
- Du C, Yao LK, Shakya S, et al. (2014) Damming of large river by debris flow: Dynamic process and particle composition. *J Mt Sci* 11(3):634-643.  
<https://doi.org/10.1007/s11629-012-2568-2>
- Gabet EJ, Mudd SM (2006) The mobilization of debris flows from shallow landslides. *Geomorphology* 74(1):207-218.  
<https://doi.org/10.1016/j.geomorph.2005.08.013>
- Gregoretti C, Fontana GD (2010) The triggering of debris flow due to channel - bed failure in some alpine headwater basins of the Dolomites: analyses of critical runoff. *Hydrol Process* 22(13):2248-2263.  
<https://doi.org/10.1002/hyp.6821>
- Ge YG, Cui P, Zhang JQ, et al. (2015) Catastrophic Debris Flows on July 10th 2013 along the Min River in Areas Seriously-hit by the Wenchuan Earthquake. *J Mt Sci* 12(1):186-206.  
<https://doi.org/10.1007/s11629-014-3100-7>
- Guo XJ, Cui P, Li Y, et al. (2016) Intensity-duration threshold of rainfall-triggered debris flows in the Wenchuan Earthquake affected area, China. *Geomorphology* 235: 208-216.  
<https://doi.org/10.1016/j.geomorph.2015.10.009>
- He YP (2003) Influence of debris flow on river channel change of Mountain River. Ph.D Thesis. Institute of mountain hazards of environment, Chinese academy of Science (In Chinese).
- Hsu L, Dietrich WE, Sklar LS (2008) Experimental study of bedrock erosion by granular flows. *J Geophys Res Earth Surf* 113 (F2): 1-21.  
<https://doi.org/10.1029/2007JF000778>
- Hu KH, Wei FQ, Li Y (2011) Real - time measurement and preliminary analysis of debris - flow impact force at Jiangjia Ravine, China. *Earth Surf Process Landf* 36(9):1268-1278.  
<https://doi.org/10.1002/esp.2155>
- Huang RQ, Pei XJ, Fan XM, et al. (2012) The characteristics and failure mechanism of the largest landslide triggered by the Wenchuan earthquake, May 12, 2008, China. *Landslides* 9:131-142.  
<https://doi.org/10.1007/s10346-011-0276-6>
- Iverson RM (1997) The physics of debris flows. *Rev Geophys* 35(3):245-296.  
<https://doi.org/10.1029/97RG00426>
- Iverson RM (2000) Landslide triggering by rain infiltration. *Water Resour Res* 36(7):1897-1910.  
<https://doi.org/10.1029/2000WR900090>
- Iverson RM, Vallance JW (2001) New views of granular mass flows. *Geology* 29(2): 115-118.  
[https://doi.org/10.1130/0091-7613\(2001\)029<0115:NVOGMF>2.0.CO;2](https://doi.org/10.1130/0091-7613(2001)029<0115:NVOGMF>2.0.CO;2)
- Iverson RM, Denlinger RP (2001) Flow of variably fluidized granular masses across three-dimensional terrain: 1. Coulomb mixture theory. *J Geophys Res solid earth* 106, 537-552.  
<https://doi.org/10.1029/2000JB900329>
- Imaizumi F, Tsuchiya S, Ohsaka O (2011) Behaviour of debris flows located in a mountainous torrent on the Ohya landslide, Japan. *Can Geotech J* 42(3): 919-931.  
<https://doi.org/10.1139/t05-019>
- Iverson RM, Reid ME, Logan M, et al. (2010) Positive feedback and momentum growth during debris-flow entrainment of wet bed sediment. *Nat Geosci* 4(2):116-121.  
<https://doi.org/10.1038/NGEO1040>
- Kang ZC, Li ZF, Ma AN, et al. (2004) Debris flow research in China. Science press (In Chinese)
- Korup O (2006) Rock-slope failure and the river long profile. *Geology* 34: 45-48.  
<https://doi.org/10.1130/G21959.1>
- Kang ZC, Cui P, Wei FQ (2006) Observation data of Dongchuan debris flow observation and research station, Chinese academy of science 1961-1984. Science press (In Chinese)
- Kean JW, Coe JA, Coviello V, et al. (2015) Estimating rates of debris flow entrainment from ground vibrations. *Geophys Res Lett* 42(15):6365-6372.  
<https://doi.org/10.1002/2015GL064811>
- Li H, Fu X, Van Der J, et al. (2008) Co-seismic surface rupture and dextral-slip oblique thrusting of the Ms 8.9 Wenchuan Earthquake. *Acta Geol Sin* 82(12): 1623-1643.  
<https://doi.org/10.4171/ZAA/949>
- Lanzoni S, Gregoretti C, Stancanelli LM (2017) Coarse-grained debris flow dynamics on erodible beds. *J Geophys Res Earth Surf* 122(3):592-614.  
<https://doi.org/10.1002/2016JF004046>
- Marchi L, Arattano M, Deganutti AM (2002) Ten years of debris-flow monitoring in the Moscardo Torrent (Italian Alps). *Geomorphology* 46(1):1-17.  
[https://doi.org/10.1016/S0169-555X\(01\)00162-3](https://doi.org/10.1016/S0169-555X(01)00162-3)
- Mcardell BW, Bartelt P, Kowalski J (2007) Field observations of basal forces and fluid pore pressure in a debris flow. *Geophys Res Lett* 34(7):1-4.

- <https://doi.org/10.1029/2006GL029183>  
Montrasio L, Valentino R, Losi G L (2009) Rainfall-induced shallow landslides: a model for the triggering mechanism of some case studies in Northern Italy. *Landslides* 6(3):241-251.  
<https://doi.org/10.1007/s10346-009-0154-7>
- Ma C, Hu KH, Tian M (2013) Comparison of debris-flow volume and activity under different formation conditions. *Nat Hazards* 67: 261-273.  
<https://doi.org/10.1007/s11069-013-0557-6>
- Ma C, Wang YJ, Hu KH, et al. (2017) Rainfall intensity-duration threshold and erosion competence of debris flows in four areas affected by the 2008 Wenchuan earthquake. *Geomorphology* 282:85-95.  
<https://doi.org/10.1016/j.geomorph.2017.01.012>
- Ma C, Deng JY, Wang R (2018) Analysis of the triggering conditions and erosion of a runoff-triggered debris flow in Miyun County, Beijing, China. *Landslides* 15(2):2475-2485.  
<https://doi.org/10.1007/s10346-018-1080-3>
- Okano K Suwa H, Kanno T (2012) Characterization of debris flows by rainstorm condition at a torrent on the Mount Yakedake volcano, Japan. *Geomorphology* 136(1):88-94.  
<https://doi.org/10.1016/j.geomorph.2011.04.006>
- Parsons J, Whipple K, Simoni A (2001) Experimental study of the grain-flow, fluid-mud transition in debris flows. *J Geol* 109(4): 427-447.  
<https://doi.org/10.1086/320798>
- Tang C, Jing Z, Ding J, et al. (2011) Catastrophic debris flows triggered by a 14 August 2010 rainfall at the epicenter of the Wenchuan earthquake. *Landslides* 8(4):485-497.  
<https://doi.org/10.1007/s10346-011-0269-5>
- Santi PM, Morandi L (2013) Comparison of debris-flow volumes from burned and unburned areas. *Landslides* 10(6):757-769.  
<https://doi.org/10.1007/s10346-012-0354-4>
- Stancanelli LM, Lanzoni S, Foti E (2015) Propagation and deposition of stony debris flows at channel confluences. *Water Resour Res* 51(7):5100-5116.  
<https://doi.org/10.1002/2015WR017116>
- Takahashi T (2007) *Debris Flows: Mechanics, Prediction and Countermeasures*, Proc. Monogr. Eng Water Earth Sci. Taylor and Francis, Leiden.  
<https://doi.org/10.1201/9780203946282>
- Tecca PR, Genevois R (2009) Field observations of the June 30, 2001 debris flow at Acquabona (Dolomites, Italy). *Landslides* 6(1):39-45.  
<https://doi.org/10.1007/s10346-009-0145-8>
- Takahashi T (2014) *Debris flow: mechanics, prediction and countermeasures*: CRC press.  
<https://doi.org/10.1201/9780203946282>
- Tang H, McGuire LA, Rengers FK, et al. (2019) Evolution of debris flow initiation mechanisms and sediment sources during a sequence of post wildfire rainstorms. *J Geophys Res Earth Surf* 124: 1572-1595.  
<https://doi.org/10.1029/2018JF004837>
- Wu JS, Kang ZC, Tian LQ (1990) Observation and research of debris flows in Jiangjia Ravine, Yunnan Province. Science press (In Chinese)
- Wei FQ, Hu KH, Cui P (2002) Characteristics and origin of debris flow of Jiangjia valley Blocking. *J Soil Water Conserv* 16(6): 71-75. (In Chinese).  
<https://doi.org/10.13870/j.cnki.stbcbx.2002.06.021>
- Zhou GGD, Ng CWW (2010) Dimensional analysis of natural debris flows. *Canadian Geotechnical Journal* 47(7):719-729.  
<https://doi.org/10.1139/T09-134>
- Zhang S, Zhang L, Chen HX, et al. (2013) Changes in runout distances of debris flows over time in the Wenchuan earthquake zone. *J Mt Sci* 10: 281-292.  
<https://doi.org/10.1007/s11629-012-2506-y>
- Zou Q, Cui P, Zhou GGD, et al. (2018) A new approach to assessing vulnerability of mountain highways subject to debris flows in China. *Prog Phys Geogr Earth Environ* 42(3): 305-329.  
<https://doi.org/10.1177/0309133318770985>
- Zhao SY, Chigira M, Wu XY (2019) Gigantic rockslides induced by fluvial incision in the Diexi area along the eastern margin of the Tibetan Plateau. *Geomorphology* 338: 27-42.  
<https://doi.org/10.1016/j.geomorph.2019.04.008>